January 2000

Surface composition of $Mn_xCo_{1-x}O$ solid solutions by X-ray photoelectron and Auger spectroscopies

Marjorie Langell
University of Nebraska - Lincoln, mlangell1@unl.edu

F. Gevrey
University of Framche Comte-Besancon, France

M. W. Nydegger
University of Nebraska - Lincoln

Published in *Applied Surface Science* 153:2–3 (January 1, 2000), pp. 114–127. doi:10.1016/S0169-4332(99)00361-X http://www.sciencedirect.com/science/journal/01694332

Submitted July 16, 1999; accepted August 21, 1999; published online December 29, 1999.

Surface composition of $Mn_xCo_{1-x}O$ solid solutions by X-ray photoelectron and Auger spectroscopies

M. A. Langell*, F. Gevrey†, and M. W. Nydegger

Department of Chemistry, University of Nebraska–Lincoln, Lincoln, NE, 68588-0303

*Corresponding author. Email: mlangell@unlinfo.unl.edu

† Present address: Department of Chemistry, University of Framche Comte-Besancon, France.

Abstract: Auger and X-ray photoelectron spectroscopies have been used to study the surface composition of $Mn_xCo_{1-x}O$ ($0 \le x \le 1$) solid solutions. The polycrystalline materials, which are bulk homogeneous, present clear signs of deviation in surface composition at $x_{bulk} \approx 0.2$–0.4 to become surface-enriched in manganese at the expense of the cobalt. Whether on stoichiometric or cobalt-depleted surfaces, cobalt retains the characteristic XPS 2p satellite structure and binding energies of the rock salt monoxide (CoO or $Mn_xCo_{1-x}O$) environment. Manganese 2p XP spectra are appropriately monoxide-like for the stoichiometric surfaces but broaden and give evidence for a second manganese species with Mn^{4+} character for the bulk-enriched samples. Oxygen O 1s spectra also show two different surface species, one the characteristic rock salt lattice oxide at 529.4 eV and a second at 531.3 eV. However, the two peaks are observed for all samples, regardless of whether the surface and bulk compositions were found to differ. The second O 1s peak cannot be unequivocally identified, but is most likely defect-oxide or hydroxyl-like in origin. The 531.3-eV O 1s species forms at the expense of the lattice oxide, and the net oxide-surface concentration is approximately that of the stoichiometric surface.

Keywords: Oxides, Solid solutions, Cobalt oxide, Manganese oxide, Defects

1. Introduction

MnO and CoO are rock salt transition metal monoxides (TMOs) with interesting electronic, magnetic and catalytic properties. The materials are also completely soluble in one another over the entire range of their mixed-metal monoxide composition, $Mn_xCo_{1-x}O$ ($0 \le x \le 1$) [1, 2] allowing their materials properties to be tailored to the task at hand. For example, an entire class of Fischer–Tropsch and oxidative-coupling catalysts relies on the chemical properties of mixed manganese monoxide–cobalt monoxide systems [3–6]. The structure of the solid solution has been shown to be homogeneous and to follow Vegard's law [1] whereby the rock salt unit cell lattice parameter shifts linearly from that of pure CoO at 4.2667 Å [7, 8a, 8b] to that of pure MnO at 4.4448 Å [7, 9a, 9b] as the composition of manganese increases from $x = 0$ to 1.

The ease of miscibility of the MnO/CoO solid solution is greatly aided by the comparable size and chemical nature of the Mn^{2+} and Co^{2+} cations in the rock salt monoxide lattice. However, both manganese and cobalt have other readily accessible oxidation states and oxide crystal structures available to them in the solid state [10], raising the question of how similar bulk and surface compositions might be for these solid solutions. For example, Co_3O_4 forms epitaxially on CoO(100) [11, 12] and both Mn_3O_4 and Mn_2O_3 form on MnO(100) [13]under very mild, UHV-accessible oxidizing conditions. In addition to phase separation, other mixed-metal manganese–cobalt oxide compositions are possible, as well. The spinel $MnCo_2O_4$ has long been known [14–17] and recent surface-sensitive analysis has shown differences in surface and bulk properties for this and similar cobalt-containing mixed-metal oxide spinel systems [18, 19]. Additional complications for the mixed-metal oxide spinel are that it appears to show variable compositional ratios for the metal cations, $Co_xMn_yO_4$, $(x + y = 3)$ [14, 15, 18, 19] and that even when "stoichiometric" at a composition of $MnCo_2O_4$ the site occupancy of the cations has been called into question, with reports that span the range from the inverse spinel structure with all Mn^{2+} in octahedral sites and the Co^{3+} divided between tetrahedral and octahedral coordination [14] to one of random octahedral/tetrahedral site occupancy and M^{2+}/M^{3+} cation oxidation states [17].

We present here surface studies on the series of polycrystalline $Mn_xCo_{1-x}O$ rock salt oxides over the entire range of bulk composition ($0 \leq x \leq 1$). The bulk is shown to be homogenous and in the correct stoichiometry by powder X-ray diffraction (XRD), with no detectable phase separation or of spinel formation. The surface composition is investigated with both Auger (AES) and X-ray photoelectron (XPS) spectroscopies, and the two techniques provide comparable results. Analysis of XPS binding energies and satellite structure for the metal 2p photoemission features are used to provide information on the chemical nature and site occupancy of the metal cation components. We find significant deviation in surface composition over some but not all of the range of the solid solution. The greatest deviation from that of the bulk appears at approximately $x = 0.2 – 0.4$ with Mn/Co ratios higher than expected due to surface segregation driven by phase separation and the apparent formation of a MnO_2-like surface phase. The surface of the solid solutions otherwise appear homogeneous and sim-

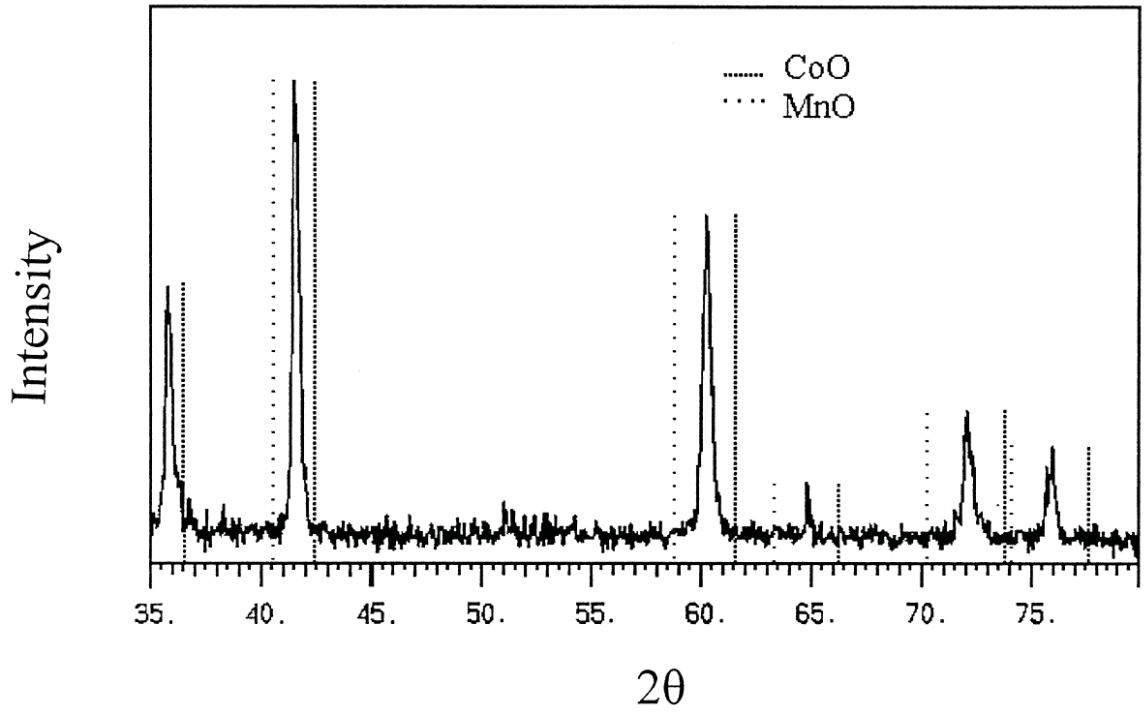

Figure 1. Powder X-ray diffraction (XRD) of the $Mn_{0.5}Co_{0.5}O$ solid solution sample, taken with Cu Kα radiation. Light dashed lines represent positions for pure MnO and heavy dashed lines represent positions for pure CoO.

ilar to that of the $Mn_xCo_{1-x}O$ bulk. As do many of the rock salt 3d TMOs, these materials have localized and highly electron-correlated band structures, which lead to characteristic peak shapes in their XP spectra. These and other effects are discussed in greater detail below.

2. Experimental

$Mn_xCo_{1-x}O$ solid solutions were prepared by mixing MnO (Alfa Aesar, 99.5% purity) with CoO (Alfa Aesar, 95%) in appropriate stoichiometric quantities to generate a series of nine samples spanning the range of concentrations $0.1 \leq x \leq 0.9$. The samples were intimately mixed by grinding with a mortar and pestle and formed into pellets to assure good physical contact of the entire sample. The pellets were then individually encapsulated in quartz tubes, which were evacuated to 3×10^{-5} Torr for several days prior to sealing. The sealed tubes were placed in a Lindberg Hevi-Duty tube furnace at 1200 K for approximately 1 week to allow the manganese and cobalt to interdiffuse to form homogeneous solutions. The homogeneity and bulk concentration of the samples were confirmed with powder XRD taken with a Rigaku Geigerflex diffractometer using Cu Kα radiation. Single-crystal substrates of MnO(100) and CoO(100) were used as reference samples for the $x = 0$ and $x = 1$ extremes of the compositional range. Their preparation and surface characterization are described more fully in [11–13].

Surface analysis of the $Mn_xCo_{1-x}O$ pellets was performed in a UHV stainless-steel bell jar, described in more detail elsewhere [20], at a base pressure of 3×10^{-10} Torr. The Auger and X-ray photoelectron spectra were acquired with a Physical Electronics (Φ) 15–255 G double-pass cylindrical mirror analyzer. AES was taken in a lock-in, derivative mode with a 2-keV primary beam energy, a scan rate of 1.0 eV/s, a modulation energy of 2

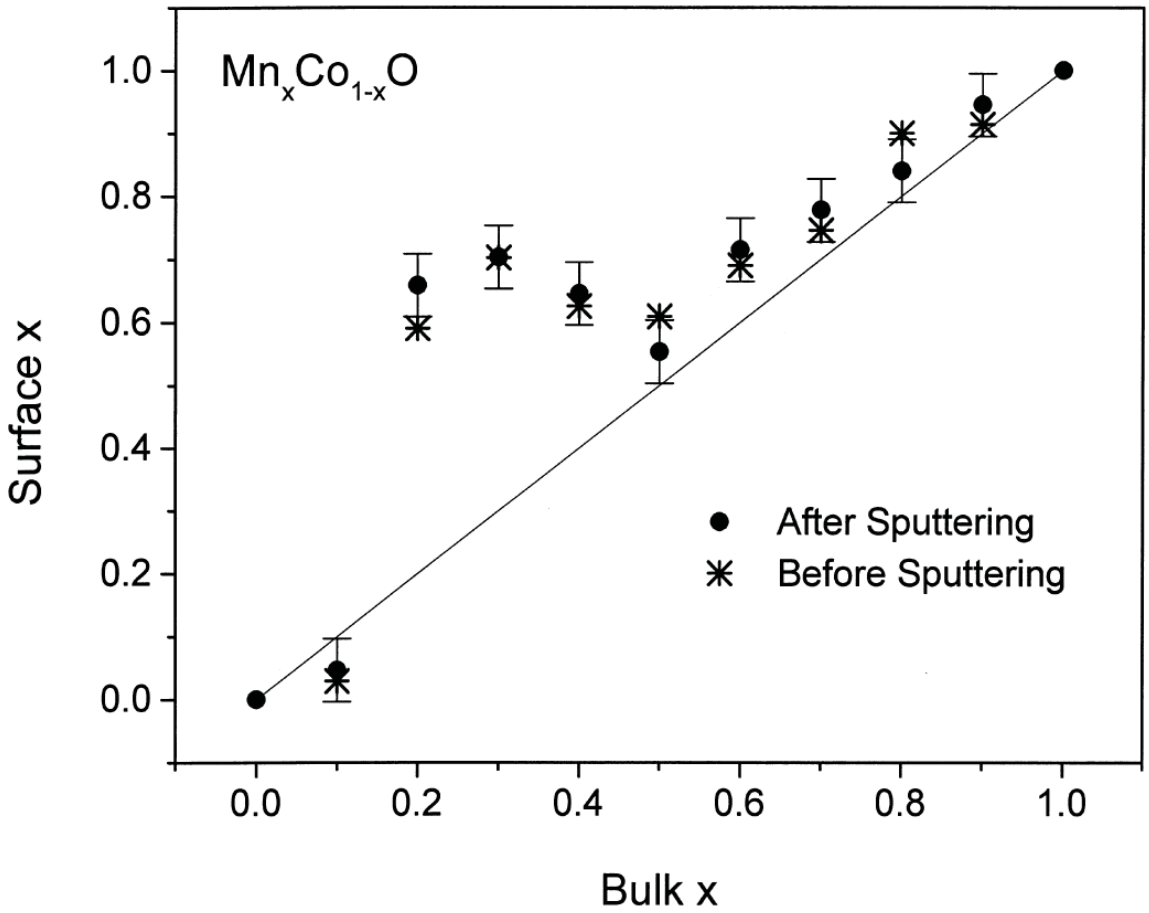

Figure 2. Auger determination of surface x composition as a function of the bulk x value for solid solutions before (*) and after (•) sputtering. For clarity, error bars are placed only on data after sputtering; data before sputtering have comparable precision.

eV and a time constant of 0.1 s. XPS was obtained in the pulse-count mode at a constant pass energy of 50 eV using Mg Kα radiation ($h\nu$ = 1253.6 eV) at 300 W. The XPS data were signal averaged for at least 200 scans and were taken in increments of 0.1 eV with dwell times of 50 ms. The samples tend to be semiconducting due to the tendency of the compound to form slightly nonstoichiometric compositions and no problems were encountered with charging in either of the electron spectroscopies used. Nevertheless, the XP binding energies were calibrated relative to the monoxide O 1s value of 529.4 eV, in agreement with values from MnO and CoO [11–13] to correct for contact potential differences between the sample and the spectrometer. No decomposition or other changes were observed in the samples during the course of the data acquisition.

Because of the small amount of carbon contamination on the as-introduced surface and the need to expose the samples briefly to atmospheric conditions in transferring the pellets from the quartz capsules to the UHV chamber, the samples were subjected to a mild argon-ion-bombardment treatment (3×10^{-5} Torr argon, 0.5 keV, 1.6 μA/cm^2 Ar^+ for 5 min). The sputtering removed the majority of carbon from the sample surface but did not otherwise significantly change the results of the analysis including composition and chemical state of the manganese, cobalt and oxygen. Both sputtered and unsputtered data are presented for compositional analysis below; other data are of the sputtered samples unless otherwise stated.

3. Results

A typical XRD for the solid solutions is shown in Figure 1 for the $Mn_{0.5}Co_{0.5}O$ sample. Samples are homogenous, rock salt materials with the appropriate lat-

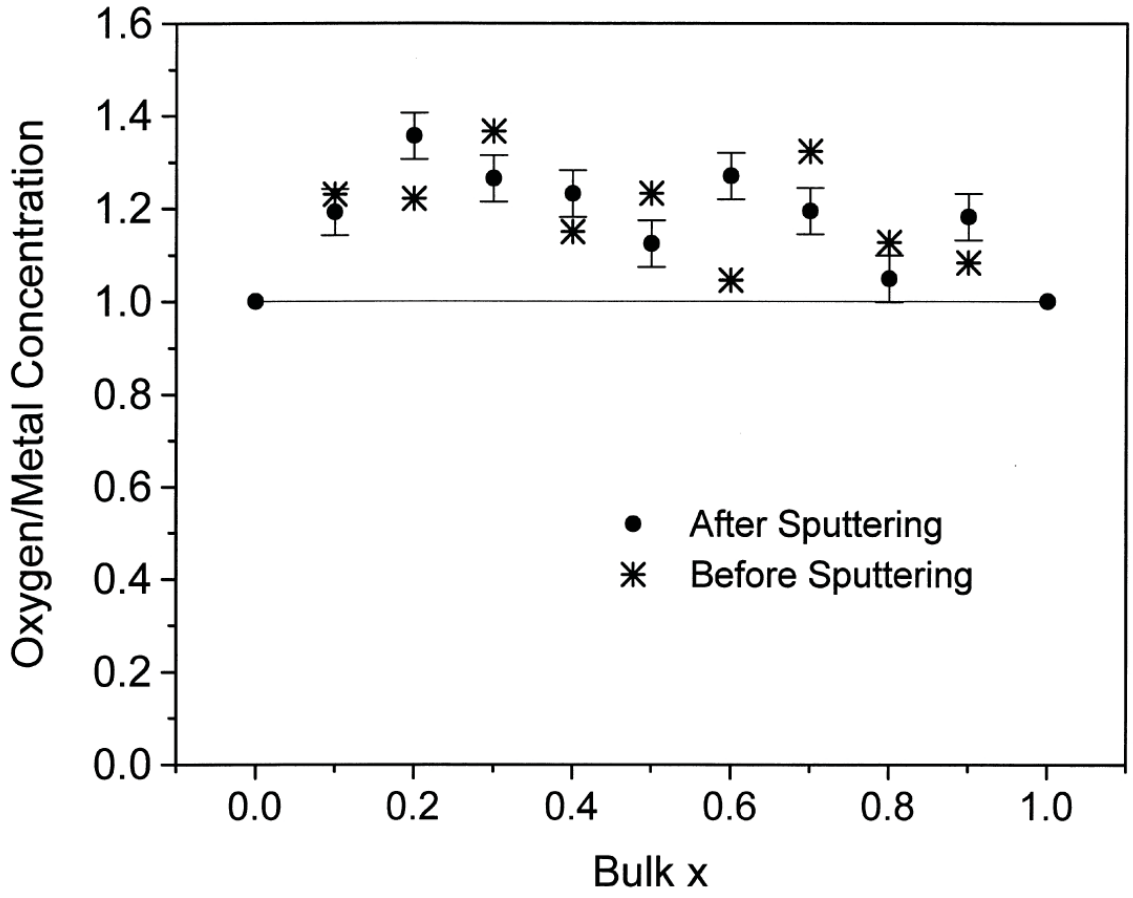

Figure 3. Auger determination of oxygen to total metal concentration ratio as a function of the bulk x value for the solid solutions before (*) and after (•) sputtering. For clarity, error bars are placed only on data after sputtering; data before sputtering have comparable precision.

tice constant. Auger analysis of the $Mn_xCo_{1-x}O$ solid solutions indicates that for very low x compositions and for $x \geq 0.5$ the surface composition mirrors that of the bulk, but that the composition deviates significantly with a maximum deviation of about $x_{surface} = 0.6$ at bulk values of $x_{bulk} = 0.2 - 0.4$. The plot of surface vs. bulk composition, shown in Figure 2, has been determined from peak-to-peak intensity values using the Auger derivative spectrum:

$$\frac{C_{Mn}}{C_{Mn} + C_{Co}} = \frac{I_{Mn}/S_{Mn}}{I_{Mn}/S_{Mn} + I_{Co}/S_{Co}} \quad (1)$$

where C_i is the surface composition of i = Mn or Co as appropriate, I_{Mn} is the peak height of the Mn $L_3M_3M_{4,5}$ Auger transition found at 589 eV, I_{Co} is the peak height of the $L_3M_{4,5}M_{4,5}$ Auger transition found at 775 eV and the S_i's are Auger sensitivity values obtained by using the MnO and CoO single-crystal data as calibration spectra. The values were obtained as a ratio, S_{Mn}/S_{Co} equal to 1.11, which is in reasonable agreement with the literature value of 1.4 obtained by interpolation of published data to that appropriate for the 2-keV primary Auger beam energy [21]. The error bars shown in the figure estimate only the uncertainty in the measured intensity ratio and do not reflect systematic errors resulting from error in the cross sections or from the simplicity of the model which assumes a homogeneous distribution of the material to within the depth sampled by the Auger measurement.

Data are shown in Figure 2 for sample surfaces both "as-introduced," with no surface pretreatment, and after the brief sputter treatment describe in the experimental section. Depending upon the sputtering efficiency, the treatment is estimated to have removed approximately 25–100 Å [22]. While the majority of carbon contamination was removed by the sputtering process, any effect on the surface concentrations of the solid solution was within error of the measurement. This indicates that the

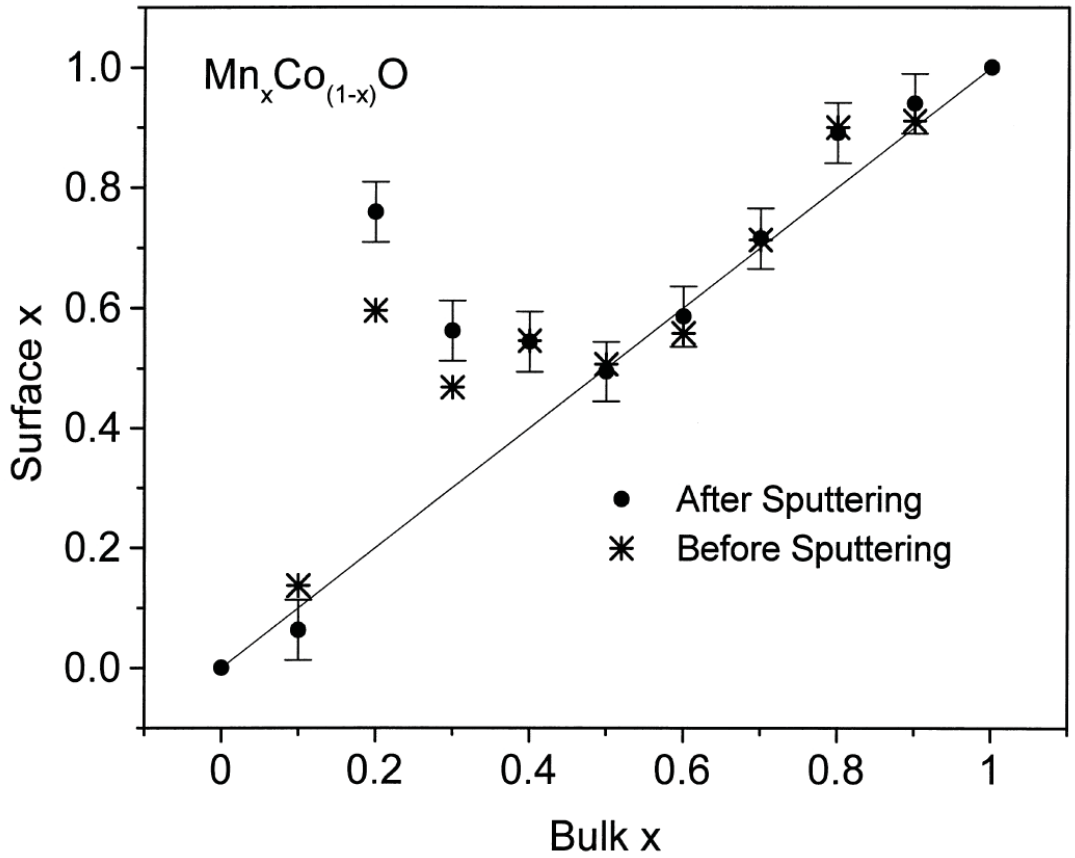

Figure 4. XPS determination of surface x composition as a function of the bulk x value for solid solutions before (*) and after (•) sputtering. For clarity, error bars are placed only on data after sputtering; data before sputtering have comparable precision.

altered concentration layer is fairly uniform within the sampling depth of the Auger analysis. It also rules out significant preferential sputtering of one metal over the other, at least at the very mild conditions (5 min of 0.5-keV Ar^+at a fluence of $\approx 5\times10^{13}$ Ar^+/cm^2s) employed in the present set of experiments. However, the parent oxides are known to undergo preferential sputtering to lose oxygen [22], which limits the usefulness of Ar^+-bombardment depth profiling with these materials, and no attempts were made to measure the actual depth of the altered layer thickness.

The oxygen (C_O) to total metal ($C_{Mn}+C_{Co}$) surface concentration can be obtained in an analogous manner:

$$\frac{C_O}{C_{Mn}+C_{Co}} = \frac{I_O/S_O}{I_{Mn}/S_{Mn}+I_{Co}/S_{Co}} \quad (2)$$

where the oxygen sensitivity factor was determined relative to that of manganese in the MnO sample to be $S_O/S_{Mn} = 2.13$. By extrapolation to the correct Auger primary beam energy, literature values place this ratio at 2.3 [21]. The data, shown in Figure 3, are in fairly good agreement with the concentration ratio slightly enriched from that expected of monoxide surface with values that average to 1.20 ± 0.07 before sputtering and 1.21 ± 0.06 after sputtering. As with the metal concentration ratios, the oxygen-to-total-metal concentration appears to remain constant after the brief Ar^+ sputter treatment. Unfortunately no trends are apparent in the data, and systematic errors result from changes in peak shape, for example, or in oxygen concentration from surface preparation factors might be significantly larger than that estimated from absolute errors in obtaining peak-to-peak Auger ratios.

Similar information on the surface concentration of the $Mn_xCo_{1-x}O$ solid solutions can be obtained with X-ray photoelectron spectroscopy. In this case, the total intensity is taken as the area under the XPS peaks for the element under analysis. Data for the metal 2p XP spectra are shown in Figure 4 to yield a plot of $x_{surface}$ as a function of x_{bulk} through use of Equation (1), similar to that obtained for the Auger data (Figure 2). The MnO and CoO single-crystal data were, again, used to obtain an XPS sensitivity factor found to be $S_{Mn}/S_{Co} = 0.57$ for the two metals. This value, which assumes that the entire 2p range is used, is comparable to a literature value of $S_{Mn}/S_{Co} = 0.68$ [23] and 0.7 [24] for Mg Kα radiation and a double-pass CMA analyzer similar to that used in the present studies. The former of these two references cautions that peak shape and cross sections for oxides tend to be variable and therefore calibration with actual CoO and MnO samples appears to be the most accurate method to within the limitations of the method. Error bars in the figure, again, reflect only the uncertainty in obtaining the intensity ratio from the XP spectrum. Because of matrix-sensitive scattering factors and other cross-sectional effects, XPS sensitivity factors are generally estimated as no more accurate than 10%–20% [25]

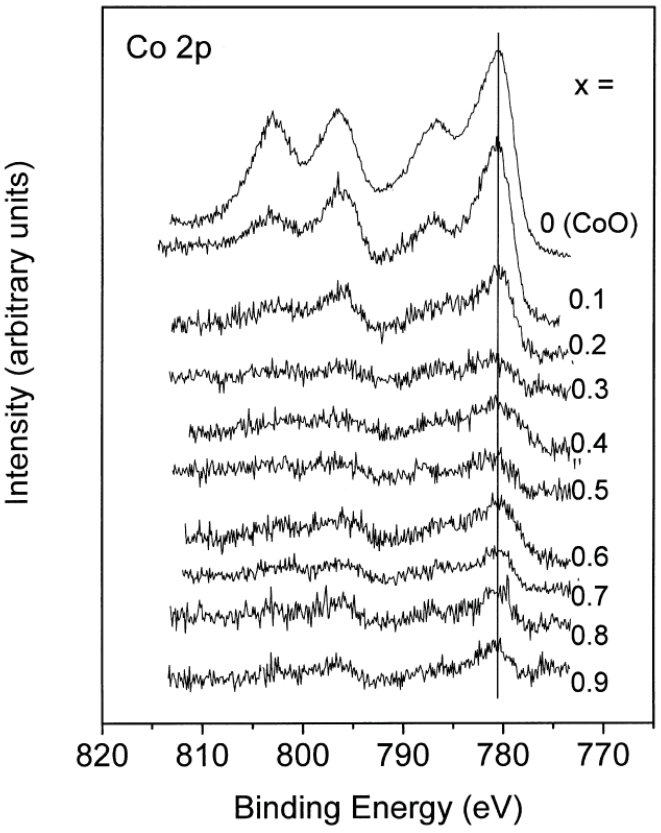

Figure 5. Cobalt 2p XP spectrum as a function of the bulk x value. Note that since the solid solution formula is given as $Mn_xCo_{1-x}O$, a smaller x value represents a larger cobalt fraction and pure CoO is represented by $x = 0$. The solid vertical line marks the peak position for the $2p_{3/2}$ transition at 780.5 eV.

and errors resulting from inhomogeneous distribution of the metals within the sampling depth of the technique cannot be estimated in the absence of additional information on the concentration profile. However, the agreement between the Auger data of Figure 2 and the XPS data of Figure 4 is very convincing of a sharp deviation in surface composition from that of the bulk in the region of $x = 0.2–0.4$.

A large amount of the variation in $x_{surface}$ from that of x_{bulk} can be explained by a substantial degree of cobalt depletion in the near-surface region. The Co 2p XP spectrum, given in Figure 5 as a function of bulk x, decreases in intensity much more rapidly than the bulk concentration particularly in the region of $x \approx 0.2–0.4$ where the greatest discrepancy in surface and bulk x-values are observed. Note that the convention for concentration is consistent with the formula $Mn_xCo_{1-x}O$ throughout this paper and, therefore, the bulk cobalt concentration in Figure 5 decreases as x_{bulk} increases (fractional Co = $1 - x$). The Co 2p binding energies and satellite structure remain the same for CoO and for all the $Mn_xCo_{1-x}O$ solid solutions, however, and are characteristic of octahedral Co^{2+}, specifically as found with the CoO rock salt electronic structure [11, 12]. Shown in greater detail in Figure 6 for the $Mn_{0.3}Co_{0.7}O$ sample, the spectrum includes Co $2p_{3/2}$ and $2p_{1/2}$ binding energies of 780.5 and 796.3 eV, respectively, along with very characteristic, intense satellites at 787.0 and 803.3 eV. The satellite structure, which is very sensitive to defects, has been shown to decrease in intensity dramatically both for relatively small increase and decrease in metal/oxygen concentration for the rock salt monoxide. Thus, while the cobalt is depleted in concentration at the surface for some bulk x values, it nevertheless retains its monoxide character throughout the entire solid solution concentration range.

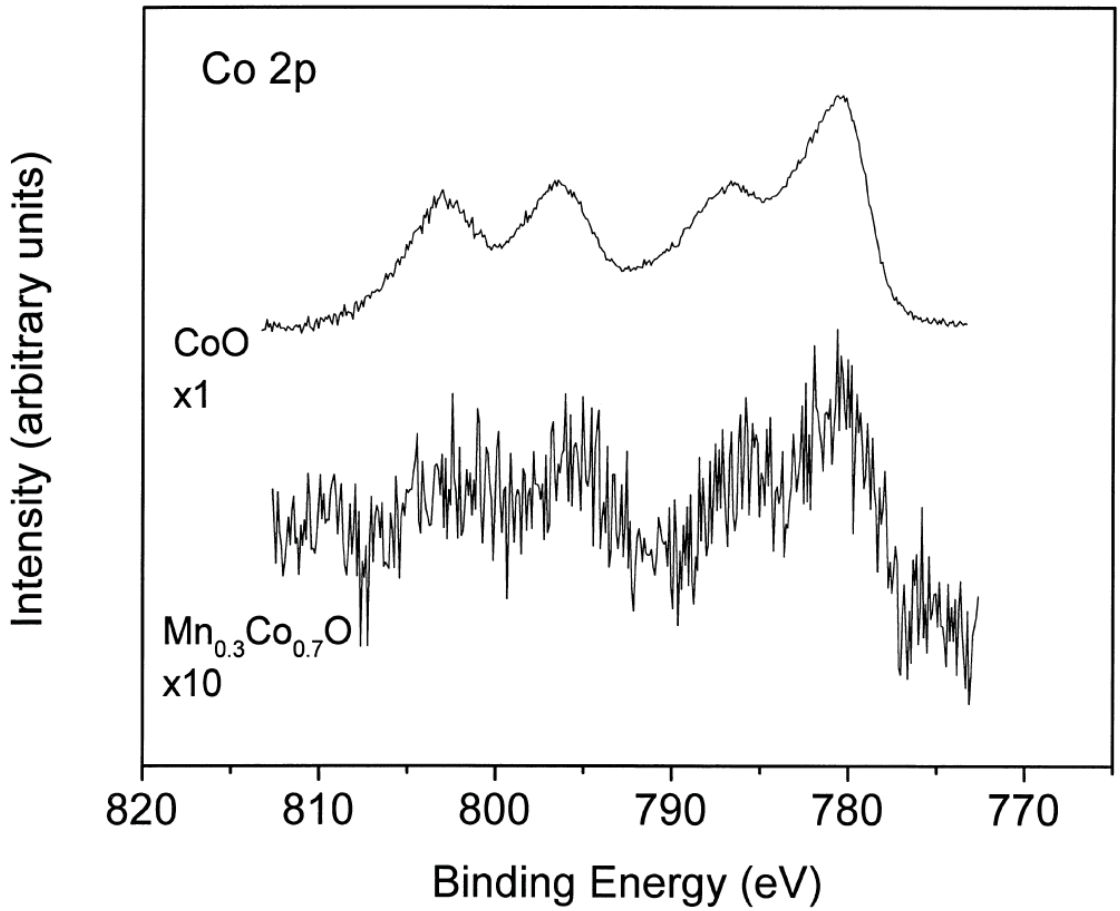

Figure 6. Co 2p XP spectrum for $Mn_{0.3}Co_{0.7}O$ compared to that of pure CoO, showing that the two have similar binding energies and intensive satellite structure expected from the rocksalt monoxide band structure. The $Mn_{0.3}Co_{0.7}O$ spectral intensity has been increased by 10× relative to that of the CoO.

Analogous Mn 2p data are shown in Figure 7. The pure MnO trace yields $2p_{3/2}$ and $2p_{1/2}$ binding energies of 640.8 and 658.7 eV, respectively, and weak satellite peaks at 647.0 eV for the $2p_{3/2}$ transition and at 658.7 eV for the $2p_{1/2}$ transition. The binding energies and spectral structure are characteristic of MnO [13, 23], which has only very weak, broad satellites in comparison to those observed for the CoO sample. Some enrichment in manganese is apparent for spectra from samples with x_{bulk} = 0.2–0.4, although more dramatic is the broadening and shift in 2p peak energies that occur for the Mn 2p spectra in this bulk concentration range. Figure 8 shows the XPS trace for the $Mn_{0.3}Co_{0.7}O$ sample, which is enriched in manganese by approximately 100% over that expected from the pure MnO spectral intensity scaled to reflect the bulk manganese composition of 0.3. Also shown in Figure 8 is the MnO spectrum adjusted in intensity to fit the leading Mn $2p_{3/2}$ edge of the $Mn_{0.3}Co_{0.7}O$ sample, and their difference spectrum. The resulting difference spectrum gives the correct $2p_{3/2}$ to $2p_{1/2}$ intensity ratio of approximately 2/1 and binding energies of 642.1 eV for $2p_{3/2}$ and 653.5 eV for $2p_{1/2}$, indicative of the formation of a higher manganese oxidation state species [23, 24, 26].

The shape of the O 1s core photoemission peak is rather complex, as is demonstrated in Figure 9 and Figure 10 for the "as-introduced" and sputtered solid solutions, respectively. In contrast to the CoO single-crystal sample, which shows a single O 1s transition at 529.4 eV with a FWHM of 2.1 eV [11, 12, 23, 24], the $Mn_xCo_{1-x}O$ solid solutions have highly variable peak widths of up to 4.0 eV FWHM and obviously represent more than one emission feature. The spectra can be curve-resolved into two individual peaks with FWHM values of 2–2.5 eV, an example of which is given in Figure 11 for the O 1s spectrum of the sputter-treated $Mn_{0.5}Co_{0.5}O$ sample. To produce this fit, a linear background was first subtracted and the spectrum was fit to two Gaussians with the restriction that the lower binding energy maximum is at 529.4 eV, as was described in the experimental section as part of the calibration procedure to the O 1s binding energy of the rock salt lattice. Fits were optimized with a least square minimization to yield $R \geq 0.99$ for all spectra and the second peak was calculated to have a binding energy of 531.31 ± 0.15 eV for the entire series.

Unlike the Auger data, a small difference in the average value of oxygen to total metal (O/M) concentration ratio is observed between the "as-introduced" and sputter-treated samples, although the difference is barely significant. Using an oxygen to manganese sensitivity ratio S_{Mn}/S_O of 4.17 obtained from the MnO single-crystal sample (S_{Mn}/S_O = 3.94, [21]) and Equation (2), O/M concentrations of 1.4±0.2 were obtained for the as-introduced samples and 0.87±0.2 for the samples after the brief sputter treatment. As was previously found with Auger analysis, the O/M concentration ratio shows no obvious trend as a function of x_{bulk}, either before or after sputtering. The O/M concentrations are shown as a function of x_{bulk} for the after-sputtered samples in Figure 12,

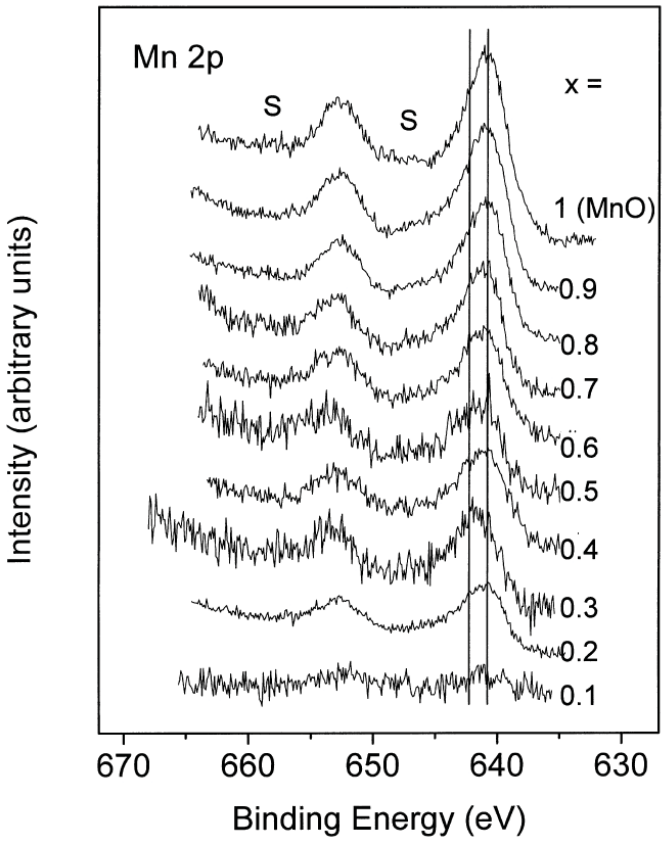

Figure 7. Mn 2p XP spectrum as a function of the bulk x value. Note that pure MnO is found for x = 1. The solid vertical lines mark the $2p_{3/2}$ peak position for each of the two species discussed in the text and are at 640.8 and 642.1 eV.

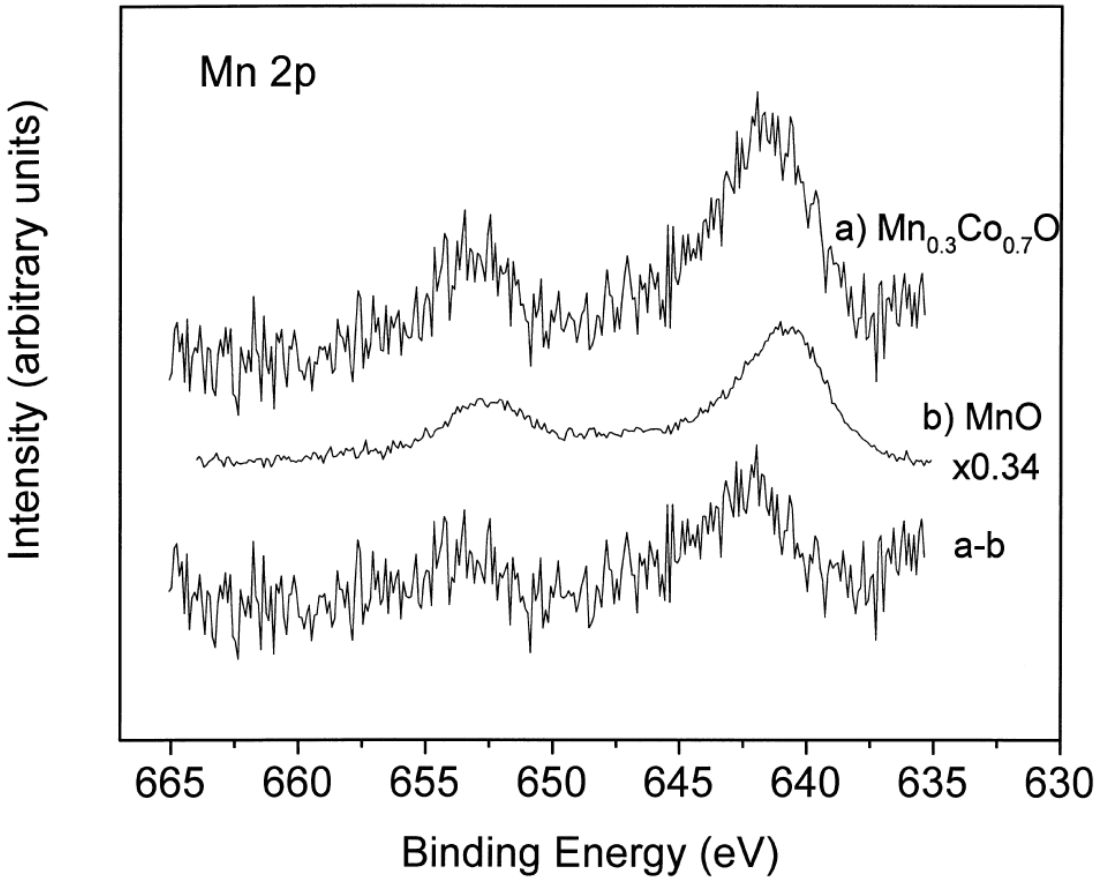

Figure 8. Illustration of the Mn 2p XPS subtraction procedure for removing the Mn^{2+}component to the $Mn_{0.3}Co_{0.7}O$ spectrum.

both for the individual 529.4- and 531.3-eV components and for the total oxygen concentration, as labeled in the figure. While some 531.3-eV component is found for all $Mn_xCo_{1-x}O$ solid solution samples, it appears to represent a larger fraction of the total near-surface oxygen for samples that also show a higher manganese/cobalt surface ratio than that expected from the bulk x values. The total oxygen concentration does not show any enrichment at these values, however, and the 531.3 eV species appears to form at the expense of the 529.4-eV lattice oxygen.

4. Discussion

Many transition metal oxides form mixed-metal oxide solid solutions over a wide range of bulk compositions. The binary rock salt monoxides, $M_xM_{1-x}'O$, often form homogeneous solutions over the entire composition range $0 \leq x \leq 1$ with lattice parameters that vary linearly with x from that of M′O to that of MO [1]. While the bulk of the material is stable as the rock salt monoxide, the surface may reflect the bulk composition over only part of the concentration range. There are several possible mechanisms for this, including surface-induced phase separation, formation of another compound such as a spinel $(M/M')_3O_4$, or preferential segregation of one component at the expense of another. Any or all of these effects might be influenced by the presence of surface impurities, either present in the bulk material or adsorbed from the ambient.

$Mn_xCo_{1-x}O$ solid solutions show evidence of manganese enrichment at low bulk manganese concentrations, approximately over the range $x_{bulk} \approx 0.2$–0.4. This may, in part, be due to the generally greater thermodynamic stability of manganese oxides relative to those of cobalt

with comparable oxygen concentrations [27]. The enrichment comes at the expense of severe cobalt depletion, and the cobalt that is detected at the surface retains XPS 2p binding energies and satellite structure characteristic of the rock salt monoxide. The peak shapes and binding energies are not compatible with Co_3O_4 [12], hydroxylated cobalt oxides [28] or $Mn_xCo_{3-x}O_4$ ($0 \le x \le 1$) spinel [18] formation. Thus, the small amount of cobalt remaining at the surface of the solid solution for $x_{bulk} \approx 0.2–0.4$ must be in the form of CoO or $Mn_xCo_{1-x}O$, and some sort of surface phase separation must have occurred.

Concurrently with the cobalt depletion, manganese 2p peak shapes broaden and, by subtracting the rock salt Mn^{2+} component, yield evidence for a second, higher binding energy species with a $2p_{3/2}$ value of 642.1 eV. In comparison with literature values, typical $2p_{3/2}$ binding energies of Mn^{3+}-containing oxides such as Mn_3O_4 and Mn_2O_3 have been reported over the range of 641.2–641.9 eV [13, 18, 24, 26, 29] whereas Mn^{4+}-containing materials are reported to be between 642.0 and 642.7 eV [18, 26, 29, 30]. High-quality thin films of epitaxially grown MnO_2 tend to have the highest binding energies and very little satellite structure [26] whereas both naturally occurring and synthetic mineral structures are represented by the lower part of the binding energy range. The minerals, synthetic or natural, contain both Mn^{4+}/Mn^{3+} to produce an average oxidation state of approximately $Mn^{3.6+}$–$Mn^{3.8+}$ [29, 30] with considerably broader 2p peaks and/or additional satellite structure. The Mn 2p binding energies and peak shapes of the second species that forms in the manganese-segregated solid solutions is closer to that observed in the variable oxidation state mineral structures.

XPS and Auger oxygen data are compatible with monoxide stoichiometry, or even with slight oxygen surface enrichment. Unfortunately, there is too much variability in oxygen intensities and too much uncertainty in

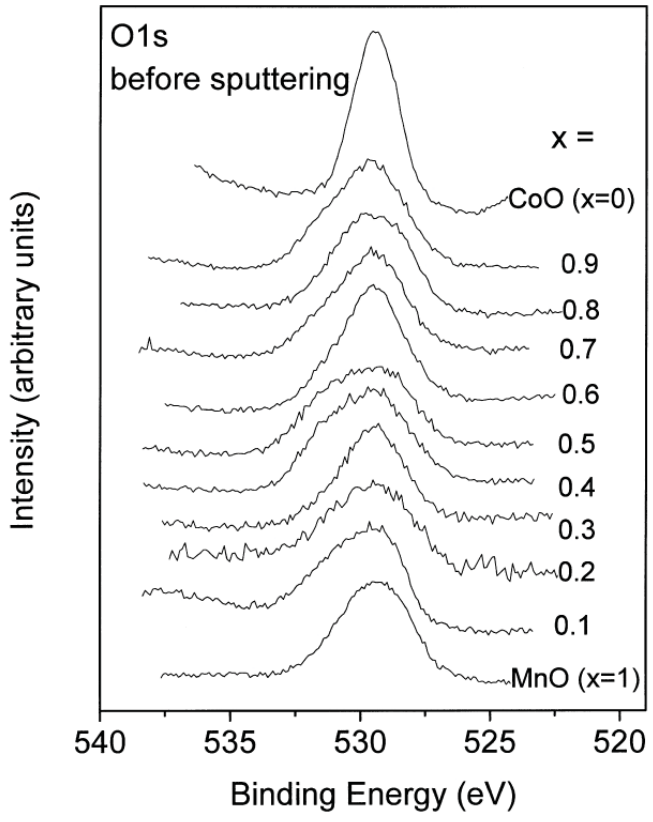

Figure 9. XP O 1s spectra as a function of bulk x for the "as-introduced" solid solutions.

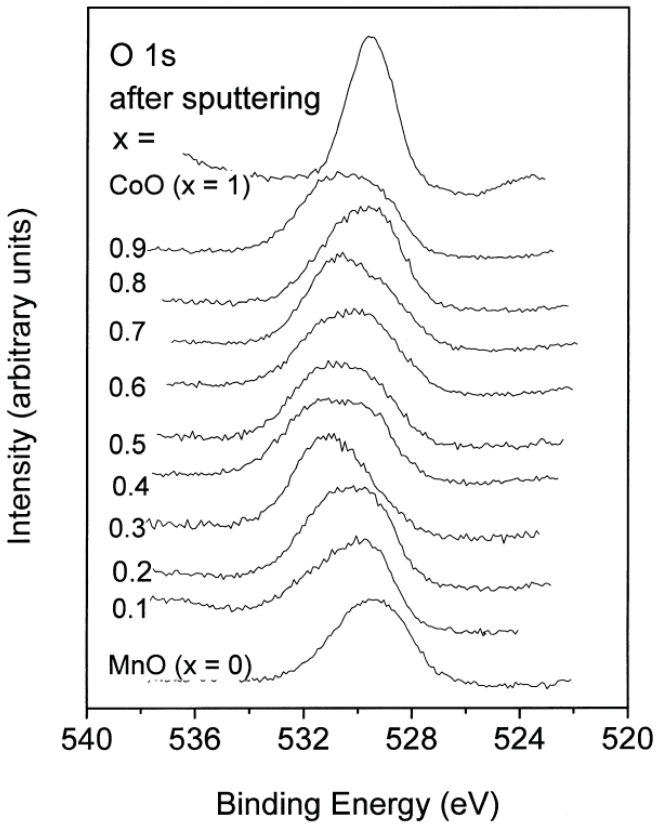

Figure 10. XP O 1s spectra as a function of bulk x for the solid solution samples after sputtering.

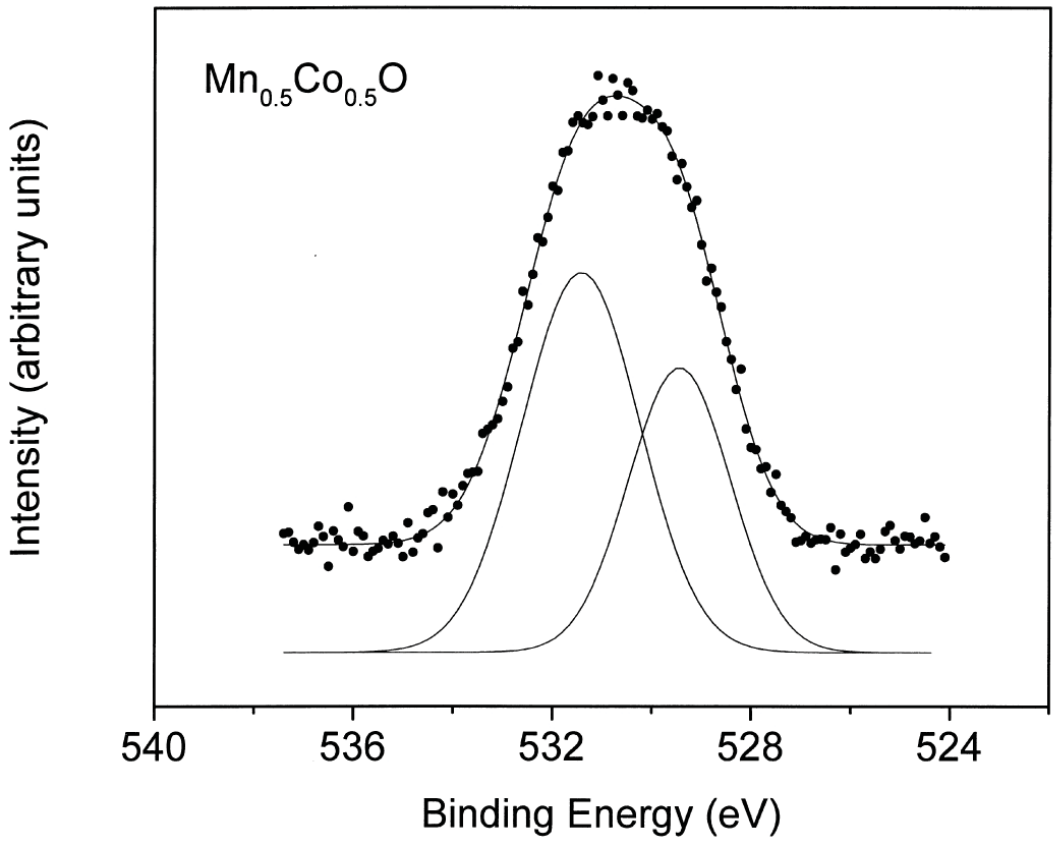

Figure 11. Illustration of the O 1s XPS fitting procedure, discussed in greater detail in the text.

converting the XPS/Auger intensities into absolute concentrations to make any strong conclusions about the net oxygen content of the surface. This is, in part, due to the tendency of oxides to gain or lose oxygen through formation of defects in the near surface, through electron or photon-stimulated desorption during data acquisition and through hydroxylation upon exposure to the ambient or even to UHV levels of background water.

Several points can be made, however, about the constitution of the O 1s photoemission peak shape. The most obvious is that the binding energy of the second peak is compatible with a very common contaminant for metal oxide surfaces. Surface hydroxyls, both those resulting from ambient adsorption and from intrinsic oxyhydroxide compositions, are typically observed at approximately this binding energy [18, 29]. However, the 531.3-eV peak is variable in concentration among the x_{bulk} compositions and actually increases in intensity for several of the x_{bulk} values upon sputtering the sample, which might otherwise have been expected to remove or at least decrease the intensity of chemisorbed impurities. Note that no bulk oxyhydroxide phases were observed in the XRD of the bulk samples. There is also a small amount of the higher-binding energy peak in the MnO spectrum, amounting to about 10% of the total O 1s intensity. This MnO(100) single-crystal surface was produced by a combination of sputter/annealing treatments [13] and, despite the presence of a small 531.3-eV component to its O 1s peak, showed no evidence of hydroxylation by high resolution electron energy loss spectroscopy (HREELS), which is able to identify surface hydroxyls definitively by the ν_{OH} vibrational loss even at low surface concentrations.

Similar high-binding energy peaks have been found for UHV studies of low P_{O2}-oxidized cobalt metal [13, 31] and cobalt monoxide [12, 32] substrates, $Ni_xCo_{1-x}O$ solid solutions [33], $Mn_xCo_{3-x}O_4$ spinel thin films formed by low-temperature spray pyrolysis [18], $La_{0.65}A_{0.35}MnO_3$ (A = Ca, Sr, Ba) giant magnetoresistance thin films [34] and Co_3O_4 single crystals cracked

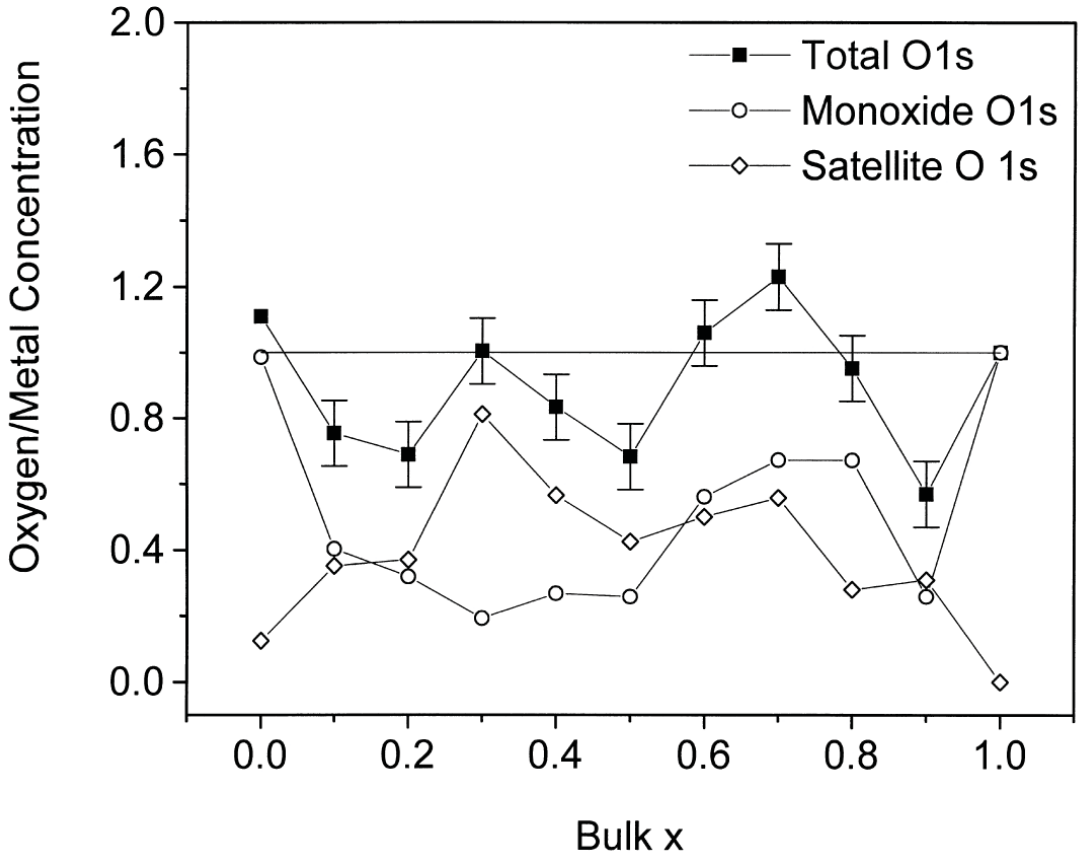

Figure 12. XPS determination of oxygen to total metal concentration ratios as a function of the bulk x for the $Mn_xCo_{1-x}O$ solid solutions after sputtering. Data include total oxygen concentration (▪), lattice oxygen 529.4 eV component (○) and "defect" 531.3 eV component (◊). For clarity, error bars are placed only on total oxygen data; other data in the plot have comparable precision.

to produce a fresh surface under UHV [35]. In addition to hydroxyl contamination resulting even from low-pressure H_2O background contaminants from the UHV chamber, the peak has been attributed to or proposed to result from nonstoichiometric near-surface oxygen [28, 30], cation defects in spinel-like near-surface layers [12, 33], phases resulting from surface segregation of one bulk metal component along with increased oxidation of the near-surface region [33] and residual signal from the templating substrate which in the case of the reported investigation happened to be SnO_2 [18]. In all these studies, the high binding energy peak looks very similar, both in terms of binding energy and relative intensity. The very intense nature indicates that, at least in the present studies, the peak is characteristic of a species that is more than simply a casual contaminant that formed on the outermost layer from UHV ambient absorption.

XPS and Auger data from this study, therefore, are compatible with phase separation into rock salt CoO or $Mn_xCo_{1-x}O$ monoxide and a Mn^{4+}-containing oxide for the part of the $Mn_xCo_{1-x}O$ solid solution range of approximately x_{bulk} = 0.2–0.4. Depending upon the actual identity of the 531.3 eV O 1s peak, the Mn^{4+}-oxide species might result from defect-like MnO_2 surface layers or might also contain a MnOOH-like species. Note that magnetic measurements have shown MnOOH to be formed from Mn^{2+}/Mn^{4+} [36] and, therefore, either defect MnO_2 or MnOOH will produce a detectable Mn^{4+} XPS signal. Hydroxylation has been found to catalyze the formation of Mn^{3+}/Mn^{4+} redox couples at the surface of $Mn_xCo_{3-x}O_4$ spinels fabricated for use as electrocatalysts [37] and the phase separation observed here may be made more favorable by the presence of surface hydroxyls as well. However, phase separation does not simply result from the presence of hydroxyls at the surface of

the solid solution, since the 531.3 eV "hydroxyl" O 1s peak is found to some extent on all of the $Mn_xCo_{1-x}O$ solid-solution surfaces, the majority of which do not differ in composition from that of their bulk.

5. Conclusion

$Mn_xCo_{1-x}O$ solid solutions have been characterized by Auger and X-ray photoelectron spectroscopies over the entire range of rock salt composition $0 \leq x \leq 1$. Mn/Co surface compositional ratios are comparable for Auger and XPS data, and show distinct signs of manganese enrichment at the expense of cobalt for the surfaces of solutions in the range $x_{bulk} = 0.2–0.4$. Oxygen intensities are more highly variable, but appear to indicate stoichiometric concentrations to slight enrichment of oxygen at the solid solution surface. Over the entire range of bulk values, cobalt shows the very characteristic 2p peak shapes and binding energies of the rock salt monoxide. Manganese 2p peaks are compatible with rock salt solid solution over much of the range studied. However for $x_{bulk} = 0.2–0.4$, where manganese enrichment occurs at the expense of cobalt, a second manganese species is observed with binding energies indicating a defect-containing Mn^{4+} oxide. O 1s XPS data also show the presence of a second species; however, this second peak is observed for all solid solutions regardless of differences found between surface and bulk metal concentrations. The deviation in surface and bulk metal concentrations found at $x_{bulk} = 0.2–0.4$ have been attributed to the formation of a more highly oxidized manganese oxide phase that contains Mn^{4+} cations. Depending on the identity of the 531.3-eV O 1s peak, this new phase is related to defect-like MnO_2 and/or MnOOH.

Acknowledgements

We gratefully acknowledge NSF for support of this project under CHE-9616690 and the State of Nebraska Research Initiative through the Center for Materials Research and Analysis.

References

1. L. Passerini. *Gazz. Chim. Ital.* **59** (1929), p. 139.
2. J. Hotzl. *Z. Phys.* **151** (1958), p. 220.
3. M.J. Keyser, R.C. Everson and R.L. Espinoza. *Appl. Catal. A* **171** (1998), p. 99.
4. G.J. Hutchings, R.G. Copperthwaite and M. Gottschalk. *J. Catal.* **137** (1992), p. 402.
5. S.E. Colley. *J. Catal.* **134** (1992), p. 186.
6. T.K. Chan and K.J. Smith. *Appl. Catal.* **60** (1990), p. 13.
7. R.W.G. Wyckoff. *Crystal Structures* Wiley, New York (1963).
8a. N.C. Tombs and H.P. Rooksby. *Nature* **165** (1950), p. 442.
8b. S. Greenwald and J.S. Smart. *Nature* **166** (1950), p. 523.
9a. C.G. Shull and J.S. Smart. *Phys. Rev.* **76** (1949), p. 1256.
9b. T.E. Moore, M. Ellis and P.W. Selwood. *J. Am. Chem. Soc.* **72** (1950), p. 856.
10. F.A. Cotton, G. Wilkinson, C.A. Murillo and M. Bochmann. *Advanced Inorganic Chemistry* (6th edn. ed.), Wiley, New York (1999).
11. M.A. Langell, G.A. Carson, M. Anderson, S. Smith and L. Peng. *Phys. Rev. B* **59** (1999), p. 4791.
12. G.A. Carson, M.H. Nassir and M.A. Langell. *J. Vac. Sci. Technol., A* **14** (1996), p. 1637.
13. M.A. Langell, C.W. Hutchings, G.A. Carson and M.H. Nassir. *J. Vac. Sci. Technol., A* **14** (1996), p. 1656.
14. P.B. Sinha and A.B. Biswas. *J. Phys. Chem. Solids* **23** (1962), p. 711.
15. P.B. Sinha, N.R. Sanjana and A.B. Biswas. *Acta Crystallogr.* **10** (1957), p. 439.
16. I. Aoki. *Arts. Sci. Chiba Univ.* **1** (1954), p. 150.
17. W.H. Cloud. *Phys. Rev.* **111** (1958), p. 1046.
18. J.L. Gautier, E. Rios, M. Gracia, J.F. Marco and J.R. Gancedo. *Thin Solid Films* **311** (1997), p. 51.
19. D. Pyke, K.K. Mallick, R. Reynolds and A.K. Bhattacharya. *J. Mater. Chem.* **8** (1998), p. 1095.
20. R.P. Furstenau, G. McDougall and M.A. Langell. *Surf. Sci.* **150** (1985), p. 55.
21. S. Mroczkowski and D. Lichtman. *J. Vac. Sci. Technol.* **3** (1985), p. 1860.
22. M.A. Langell. *Surf. Sci.* **186** (1987), p. 323.
23. D. Briggs and M.P. Seah. In: (2nd edn. ed.),*Practical Surface Analysis* **1** Wiley, New York (1990), p. 641.
24. C.D. Wagner, W.M. Riggs, L.E. Davis, J.F. Moulder and G.E. Muilenberg. In: *Handbook of X-Ray Photoelectron*

Spectroscopy Physical Electronics Industries, Eden Prairie, MN (1979), p. 188.

25. S. Tougaard. *Surf. Interface Anal.* **25** (1997), p. 137.
26. S.A. Chambers and Y. Liang. *Surf. Sci.* **420** (1999), p. 123.
27. I. Barin and O. Knacke. *Thermochemical Properties of Inorganic Substance* Springer-Verlag, New York (1973).
28. C.R. Brundle, T.J. Chuang and D.W. Rice. *Surf. Sci.* **60** (1976), p. 286.
29. H.W. Nesbitt and D. Banerjee. *Am. Mineral.* **83** (1998), p. 305.
30. S. Ching, D.J. Petrovay, S. Suib, Inorganic Chem., 36 (1007) 883..
31. M. Oku and Y. Sato. *Appl. Surf. Sci.* **55** (1992), p. 37.
32. B.W. Lee, A. Ignatiev, J.A. Taylor and J.W. Rabalais. *Solid State Commun.* **33** (1980), p. 1205.
33. M.W. Nydegger, G. Couderc and M.A. Langell. *Appl. Surf. Sci.* **147** (1999), p. 58.
34. J.-W. Choi, H. Dulli, Y. Feng, S.-H. Liou, P.A. Dowben and M.A. Langell. *Phys. Status Solidi B* **214** (1999), p. 45.
35. D. Pugmire, W. McCarroll, M.A. Langell, unpublished results..
36. F.A. Cotton and G. Wilkenson. In: *Advanced Inorganic* (3rd edn. ed.), Interscience Publishers, New York (1972), p. 849.
37. E. Rios, J.-L. Gautier, G. Poillerat and P. Chatier. *Electrochim. Acta* **44** (1998), p. 1491.